Quantum criticality of a $\mathbb{Z}_3$-symmetric spin chain with long-range interactions

Xue-Jia Yu,[1] Chengxiang Ding,[2] and Limei Xu[1,3,4,*]

[1]*International Center for Quantum Materials, School of Physics, Peking University, Beijing 100871, China*
[2]*School of Science and Engineering of Mathematics and Physics, Anhui University of Technology, Maanshan, Anhui 243002, China*
[3]*Collaborative Innovation Center of Quantum Matter, Beijing, China*
[4]*Interdisciplinary Institute of Light-Element Quantum Materials and Research Center for Light-Element Advanced Materials, Peking University, Beijing, China*

(Received 24 January 2023; accepted 28 April 2023; published 19 May 2023)

Based on large-scale density matrix renormalization group techniques, we investigate the critical behaviors of quantum three-state Potts chains with long-range interactions. Using fidelity susceptibility as an indicator, we obtain a complete phase diagram of the system. The results show that as the long-range interaction power α increases, the critical points f_c^* shift towards lower values. In addition, the critical threshold $\alpha_c(\approx 1.43)$ of the long-range interaction power is obtained for the first time by a nonperturbative numerical method. This indicates that the critical behavior of the system can be naturally divided into two distinct universality classes, namely the long-range ($\alpha < \alpha_c$) and short-range ($\alpha > \alpha_c$) universality classes, qualitatively consistent with the classical ϕ^3 effective field theory. This work provides a useful reference for further research on phase transitions in quantum spin chains with long-range interaction.

DOI: 10.1103/PhysRevE.107.054122

I. INTRODUCTION

Quantum phase transitions (QPTs) are phase transitions between quantum matters at zero temperature by tuning athermal parameters, which can be a first-order phase transition represented by some sudden abrupt jump behavior or a continuous phase transition described by a critical exponent. Universality class categorized by critical points or unstable fixed points in the sense of renormalization group (RG) [1] is a core concept in QPTs. Using field theory or numerical exact approaches, conventional or unconventional QPT can be described by constructing simplified effective lattice models [2–4]. Therefore, quantum many-body systems with nearest-neighbor interactions, such as the transverse field Ising model, Heisenberg model, and Hubbard model, are of fundamental importance for understanding QPTs and universality classes [5]. A well-known QPT is the second-order Ising transition in the one-dimensional transverse field Ising model, and its critical exponents are perfectly supported by experimental results [5].

Quantum systems with long-range interactions, such as Coulomb interaction $(1/r_{ij})$ [6], dipole-dipole interaction $(1/r_{ij}^3)$ [7,8], and van der Waals interaction $(1/r_{ij}^6)$ [6], have attracted widespread attention in recent years, accompanied by significant advances in experimental techniques for manipulating quantum simulators, such as atomic, molecular, and optical systems [6,8–11]. For instance, tunable power-law interactions $1/r^{d+\alpha}$ with a power $0 \leqslant \alpha + d \leqslant 3$ are realized in trapped ions [12–16], which provides a perfect platform for studying novel physics of quantum many-body systems with long-range power-law interaction and stimulated many subsequent many-body physics studies. One example is the neutral Rydberg atom trapped in optical tweezers with programmable van der Waals interactions. It provides promising tunable platforms to explore various novel physics, such as gapped $\mathbb{Z}_2$ quantum spin liquids [17–23], quantum phase transitions between different density wave ordered (e.g., $\mathbb{Z}_3$ ordered) and disordered phases [24–31]. Specifically, the $\mathbb{Z}_n$-symmetric quantum spin model system [32,33], namely the "parafermion" model system, favors topological phases with more efficient non-Abelian anyon bound states [32,33], providing a possible approach for universal topological quantum computing, thereby attracting extensive attention and stimulated extensive studies [33–40]. However, despite extensive interest in $\mathbb{Z}_n$-symmetric quantum many-body systems with long-range interactions, it remains challenging to fully understand their critical behavior both theoretically and numerically.

It is well known that a d dimensional quantum system with short-range interactions has a well-known equivalent classical counterpart in $d+1$ dimensions. However, the quantum system with long-range interactions does not have a direct counterpart due to the subtle relationship between classical and quantum critical behaviors. For classical O(N) or $\mathbb{Z}_n$-symmetric spin model systems with long-range interactions [41–50], previous RG calculations show that according to the interaction power α, the critical behavior falls into three university classes, namely, (i) the mean-field universality class when $\alpha \leqslant d/2$, (ii) the long-range universality class when $d/2 < \alpha \leqslant \alpha_c$, and (iii) the short-range universality class for $\alpha > \alpha_c$. Note that region (ii) is a "nonclassical" region where the critical behavior is characterized by a peculiar long-range critical exponent $\alpha_c(=2-\eta_{SR})$, which can be predicted by

*limei.xu@pku.edu.cn

perturbative RG calculations with a short-range anomalous exponent η_{SR} [41,45]. The quantum three-state Potts chain is the simplest example of "parafermion" systems, which shows a continuous phase transition from "topological phase" (Potts ordered) to trivial phase (disordered), thereby is of crucial importance for quantum computing [32,33,51,52]. The question is what is the critical behavior of such quantum Potts chains with long-range interaction in the "nonclassical" region, and how to estimate the critical exponent α_c if there is a long-range to short-range universality class crossover.

Fidelity susceptibility is a purely geometric quantity of quantum states from quantum information world with an obvious advantage that no prior knowledge of order parameters and symmetry breaking is required. It has been applied to detect a wide range of QPTs [53–64] induced by a sudden change in the structure of the wave function. The fidelity susceptibility, defined as the response of the wave-function overlap of two neighboring ground states with respect to an external field, diverges at the critical point and is almost zero away from the critical point, thus characterizing the QPTs well. For example, experiments detect the QPTs in terms of fidelity susceptibility by using the neutron scattering or angle-resolved photoemission spectroscopy (ARPES) techniques [65]. However, there is also some work [66–68] showing that fidelity susceptibility does not diverge for high-order phase transitions. Here, we investigate the finite-size scaling behavior of the fidelity susceptibility [67,69–71] in the quantum Potts chain with long-range interactions using the finite-size density-matrix renormalization-group (DMRG) method [72–74] based on the matrix product states (MPS) [74,75]. The critical long-range interaction power α_c is determined in a nonperturbative way for the first time, providing important insight into phase transitions of quantum spin chains with long-range interaction.

The rest of this paper is organized as follows: Sec. II contains the lattice model of the quantum Potts chain with long-range power-law interaction, the numerical method employed, and the scaling relations of fidelity susceptibility. Section III shows the phase diagram of the quantum Potts chain with long-range interaction and the finite-size scaling of the critical behavior, followed by a brief discussion in comparison with previous two-loop RG results. The conclusion is presented in Sec. IV. Additional data for our numerical calculations are provided in the Appendixes.

II. MODEL AND METHODS

A. Quantum Potts chain with long-range interaction

The system of our study is a quantum three-state Potts chain with long-range power-law interactions [see Fig. 1(a)], described by the following Hamiltonian [76,77]:

$$H_{\mathrm{LRP}} = H_0 + fH_1 = -\frac{J}{N(\alpha)}\sum_{i,j}\frac{(\sigma_i^\dagger\sigma_j + \sigma_i\sigma_j^\dagger)}{|i-j|^{d+\alpha}} - f\sum_i(\tau_i + \tau_i^\dagger), \quad (1)$$

where H_1 and H_0 are the driving and undriving Hamiltonian, respectively. J is the interaction strength, and f represents the external transverse field, parameter α tunes the power of

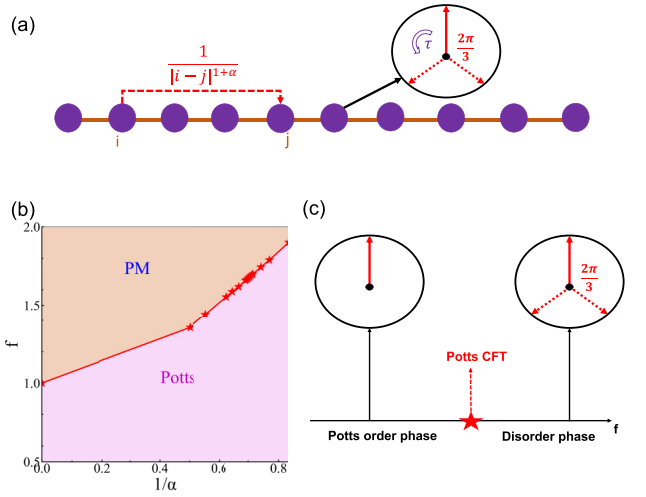

FIG. 1. Schematic long-range interaction (a) and ground-state phase diagram with respect to $1/\alpha$ and external transverse field f of the quantum Potts chain with long-range interaction (b). In (b), Potts donates the Potts order phase. PM denotes the paramagnetic disorder phase (see the main text). The red line is the phase boundary between the Potts and PM phases, and red star symbols denote the DMRG results of the critical values f_c^*. (c) The schematic phase diagram of the standard quantum Potts chain with the nearest-neighboring interaction. The critical point between the Potts ordered phase and disordered phase belongs to Potts universality class, which is described by Potts CFT.

long-range interactions ($\frac{1}{|i-j|^{d+\alpha}}$), and d is the spatial dimension (equal to 1 in our case). $N(\alpha)(=\frac{1}{N-1}\sum_{i,j,i\neq j}\frac{1}{r_{ij}^{\alpha}})$ is the Kac factor to preserve the Hamiltonian extensive. σ dictates the direction of the watch hand, and τ rotates the watch hand clockwise through a discrete angle $2\pi/3$, as shown in Fig. 1(a). σ and τ satisfy $\sigma_i^3 = I$, $\tau_i^3 = I$, and $\sigma_i\tau_j = \omega\delta_{ij}\tau_j\sigma_i$, where $\omega = e^{2\pi i/3}$. A global $\mathbb{Z}_3$ transformation represented by $G = \prod_i \tau_i$ makes the Hamiltonian invariant. The operators are defined by

$$\sigma = \begin{pmatrix} 1 & 0 & 0 \\ 0 & \omega & 0 \\ 0 & 0 & \omega^2 \end{pmatrix}, \quad \tau = \begin{pmatrix} 0 & 1 & 0 \\ 0 & 0 & 1 \\ 1 & 0 & 0 \end{pmatrix}. \quad (2)$$

The system is in an ordered phase which breaks the $\mathbb{Z}_3$ symmetry for $f \ll J$ and in a disordered paramagnetic phase (PM) for $f \gg J$. The phase transition from the $\mathbb{Z}_3$-breaking Potts order to the $\mathbb{Z}_3$-symmetric disordered phase is described by the three-state Potts CFT with correlation length exponent $\nu = 5/6$. The model becomes an infinite-range Potts chain (Lipkin-Meshkov-Glick model [78]) when $\alpha + d = 0$, and a nearest-neighbor quantum Potts chain when $\alpha + d = \infty$.

Nonperturbative numerical methods are employed to investigate critical behaviors of quantum Potts chains with long-range power-law interaction and estimate the value of α_c in the "nonclassical" region. Since this region has been estimated from two-loop RG calculations [45], we only consider $1.2 \leqslant \alpha \leqslant 2.0$. Considering that the quantum Potts chain with long-range interaction does not have exact solutions in the parameter region of interest, a large-scale finite-size DMRG

method [72–74] based on MPS [74,75], which is one of the most powerful numerical methods for one-dimensional strongly correlated many-body systems, is employed. The MPS bond dimension is set to 300; good convergence of true energy eigenstates and fidelity susceptibilities are guaranteed by requiring relative energy errors less than 10^{-8}. The fidelity susceptibility defined in Eq. (3) is computed with a minimal step $\delta f = 10^{-3}$. We chose the same initial state in the DMRG calculations every time, so the ground states in the ordered phase are the same. The strength of the interaction $J = 1$ as an energy unit, and open boundary conditions are applied.

B. Fidelity susceptibility and scaling relations

The system undergoes a continuous phase transition from an ordered to a disordered phase when tuning the external field f to a critical value f_c^*, at which the structure of the ground-state wave function changes significantly. The quantum ground-state fidelity $F(f, f+\delta f)$, defined as the overlapping amplitude of the ground-state wave function with the external field f and the ground-state wave function with the external field $f+\delta f$ [65,67,69–71,79], and its value is almost zero near f_c^*, that is, $F(f_c^*, f_c^*+\delta f) \sim 0$. In practice, the more convenient quantity to characterize QPTs is the fidelity susceptibility, defined by the leading term of the fidelity,

$$\chi_F(f) = \lim_{\delta f \to 0} \frac{2(1 - F(f, f+\delta f))}{(\delta f)^2}. \tag{3}$$

For a continuous quantum phase transition of a finite system with size L, fidelity susceptibility exhibits a peak at pseudocritical point $f_c(L)$, and the value of the quantum critical point f_c^* can be estimated by polynomial fitting $f_c(L) = f_c^* + aL^{-1/\nu}$ [80]. In the vicinity of $f_c(L)$, previous studies [53–58,62,65,69] have shown that the finite-size scaling behaviors of fidelity susceptibility $\chi_F(f)$ follows:

$$\chi_F(f \to f_c(L)) \propto L^{\mu}, \tag{4}$$

and

$$L^{-d}\chi_F(f) = L^{(2/\nu)-d} f_{\chi_F}(L^{1/\nu}|f - f_c^*|), \tag{5}$$

where $\mu(=2+2z-2\Delta_V)$ is the critical adiabatic dimension [69]. Δ_V is the scaling dimension of the local interaction $V(x)$ at f_c^*, ν is the critical exponent of the correlation length, and it can be easily computed according to the relation: $\nu = 2/\mu$. z is the dynamic exponent, d is the spatial dimension of the system, and f_{χ_F} is an unknown scaling function. Based on Eq. (4), the values of critical exponents ν and μ of the QPT can be determined, and critical behavior of the long-range quantum system can be easily determined. Note that in practice, the critical exponent μ is usually extracted from fidelity susceptibility per site, $\chi_L(f) = \chi_F(f)/L^d$.

III. PHASE DIAGRAM AND CRITICAL BEHAVIOR

A. Quantum phase diagram

The ground-state phase diagram of the quantum Potts chain with long-range interactions for $\alpha > 0$ [Eq. (1)] is obtained by performing large-scale DMRG simulations with $L = 96, 120, 144, 156, 168, 192, 216, 240$ sites. The result is presented in Fig. 1(b). For $\alpha \to \infty$, the ground state is a Potts order phase with three-fold degeneracy for $f = 0$ and a paramagnetic disorder phase for $f \to \infty$, consistent with previous results [37] [also see Fig. 1(c)]. Furthermore, for finite α, it is found that the quantum Potts chain with long-range interactions has a stable Potts order and a disordered phase over the entire range of α we investigate.

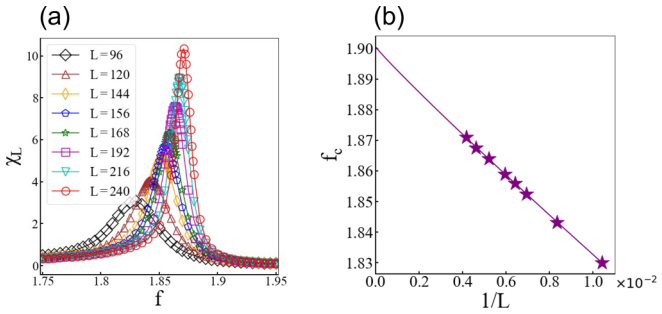

FIG. 2. (a) Fidelity susceptibility per site χ_L of the Potts chain with long-range interaction for $\alpha = 1.2$ and $L = 96, 120, 144, 156, 168, 192, 216, 240$ sites as a function of external transverse field f; symbols denote finite-size DMRG results. (b) Extrapolation of critical point f_c^* for the Potts chain with long-range interaction; symbols denote the finite-size DMRG results for $\alpha = 1.2$ and $L = 96, 120, 144, 156, 168, 192, 216, 240$ sites. We use polynomial fitting $f_c(L) = f_c^* + aL^{-1/\nu}$ and extrapolate the critical point $f_c^* = 1.901 \pm 0.002$.

The finite-size scaling behavior of fidelity susceptibility for $\alpha = 1.2$ with different L is presented in Fig. 2(a), which obeys $\chi_L(f_c(L)) \propto L^{\mu-1}$ [Eq. (4)] near the second-order QPT critical point. As system size L increases, the peak position $f_c(L)$ gets closer and closer to the exact critical point value f_c^*. More precisely, for the long-range interaction Potts chain with $\alpha = 1.2$, f_c^* is determined by polynomial fitting $f_c(L) = f_c^* + aL^{-1/\nu}$, and then extrapolating to L to infinity [Fig. 2(b)]. According to Eq. (5), the fidelity susceptibility follows an exact scaling relation, and collapses to one master curve [Fig. 3(b)], confirming that the extrapolation is appropriate. The finite-size scaling behavior of fidelity susceptibility for other α is also investigated (see Appendix A), and the results are presented in Table I. Results show that the quantum critical point moves to lower f_c^* values as α increases.

B. Finite-size scaling and critical exponent

The next questions are what is the critical behavior of the long-range interaction Potts chains with different α values, and whether there is a critical threshold α_c, at which the critical behavior changes continuously from a long-range universality class to a short-range one? To this end, we calculate the critical exponents μ and ν of the fidelity susceptibility in the region $1.2 \leqslant \alpha \leqslant 2.0$ based on large-scale DMRG simulations for different L. The value of the fidelity susceptibility per site, $\chi_L = \chi_F/L$, at the peak position $f_c(L)$ for different L at $\alpha = 1.2$ is shown in Fig. 3(a). The adiabatic critical dimension μ can be well fitted by a polynomial fitting of $\chi_L(f_c(L)) = L^{\mu-1}(c + dL^{-1})$.

According to Eq. (5), the fidelity susceptibility can be scaled by $L^{-2/\nu}\chi_F$ as a function of $L^{1/\nu}(f - f_c^*)$ in the

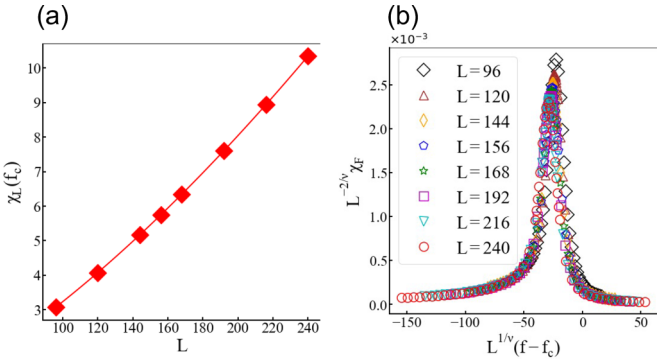

FIG. 3. (a) The maximal of fidelity susceptibility per site $\chi_L = \chi_F/L$ as a function of system sizes L for $\alpha = 1.2$. We use polynomial fitting $\chi_L(f_c(L)) = L^{\mu-1}(c + dL^{-1})$ and extrapolate the critical adiabatic dimension $\mu = 2.54 \pm 0.02$. (b) Data collapse of fidelity susceptibility χ_F for the Potts chain with long-range interaction; symbols denote the finite-size DMRG results for $\alpha = 1.2$ and $L = 96, 120, 144, 156, 168, 192, 216, 240$ sites, where $\nu = 0.791 \pm 0.004$ and $f_c^* = 1.901 \pm 0.002$ are used for data collapse plots.

vicinity of the quantum critical point f_c^*. The critical correlation length exponent ν is then determined by $\nu = 2/\mu$. Put the obtained critical point f_c^* and critical exponent ν into Eq. (5), all fidelity susceptibilities for different L collapse into a single one [Fig. 3(b)], which means the estimated critical point and critical exponent are accurate. We also noticed that the data collapse peak is not at 0 because of the finite-size effect for $f(L) = f_c^* + aL^{-1/\nu}(a \neq 0)$. The calculations of the critical adiabatic dimension μ and the correlation length exponent ν for other α are presented in Appendix C, and the results of all α are summarized in Table I. As can be seen from Fig. 4(a), either ν or μ as a function of $1/\alpha$ shows a crossover at $1/\alpha = 1/\alpha_c = 0.699(\alpha_c = 1.43)$. When $\alpha < \alpha_c$, μ and ν are monotonic functions of α. In contrast, when $\alpha > \alpha_c$, they are more or less constant and approach the critical exponent

TABLE I. Critical exponents of the Potts chain with long-range interaction for different α. Critical exponents in the standard quantum Potts chain ($\alpha = \infty$) are also listed for comparison. The critical threshold of long-range interaction power $\alpha_c \sim 1.43$.

α	f_c^*	ν	μ
1.2	1.901(2)	0.791(4)	2.54(2)
1.3	1.7888(8)	0.804(2)	2.488(5)
1.35	1.744(1)	0.813(3)	2.46(1)
1.4	1.699(1)	0.827(4)	2.42(1)
1.41	1.692(2)	0.8292(7)	2.412(2)
1.42	1.683(2)	0.833(2)	2.402(4)
1.43	1.6742(7)	0.8337(7)	2.399(2)
1.44	1.6663(6)	0.837(2)	2.391(4)
1.45	1.659(1)	0.839(3)	2.385(6)
1.5	1.6191(7)	0.841(3)	2.380(8)
1.55	1.588(1)	0.840(2)	2.382(5)
1.6	1.554(2)	0.843(3)	2.374(7)
1.8	1.4416(4)	0.843(1)	2.373(2)
2.0	1.3541(7)	0.840(2)	2.381(6)
∞	1.00000	0.83333	2.40000

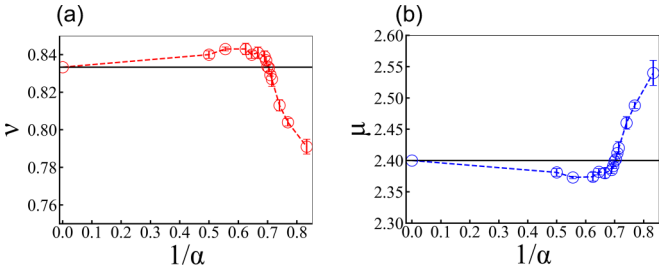

FIG. 4. Critical exponent of the correlation length ν (black dash line refers to 2D three-state Potts correlation length exponent $\nu = 5/6$ as a comparison) (a) and critical adiabatic dimension μ (black dash line refers to 2D three-state Potts critical adiabatic dimension $\mu = 12/5$ as a comparison) (b) with respect to $1/\alpha$ for the Potts chain with long-range interaction; the symbols denote the finite-size DMRG results that are obtained by extrapolating from the fidelity susceptibility $\chi_F(f_c(L))$ at the peak position $f_c(L)$ of $L = 96, 120, 144, 156, 168, 192, 216, 240$ sites.

values of the two-dimensional (2D) three-state Potts model, $\nu = 5/6$ and $\mu = 12/5$, respectively, within 0.8% error due to finite-size effect (black dash line in Fig. 4). Therefore, the critical behavior of the fidelity susceptibility undergoes a continuous crossover at $\alpha_c \approx 1.43$, from the long-range universality class region with varying correlation length exponent ($\alpha < \alpha_c$) to the short-range universality class region with constant exponents ($\alpha > \alpha_c$, three-state Potts region). This tendency is different from $\boldsymbol{Z}_2$-symmetric (Ising) quantum spin chain with long-range interaction [81,82].

C. Discussion

The application of RG techniques to *classical* spin systems with long-range interactions provides a good understanding of phase transitions that occur within them. Perturbative two-loop RG calculations show that the three-state Potts chain with long-range power-law interactions has three parameter regimes: (i) small α ($\alpha < d/2$), (ii) intermediate $\alpha(d/2 < \alpha < \alpha_c$, and (iii) large $\alpha(\alpha > \alpha_c)$ regions, similar to the classical three-state Potts model at low energy and long distance that can be described by ϕ^3 Landau-Ginzberg-Wilson effective action [44,45]. Moreover, previous theoretical and numerical results [41,43,81,82] show that the critical behavior of O(N) symmetric *quantum* model systems with long-range interactions is consistent with that of *classical*O(N) ones with effective dimension $d_{\text{eff}}(=\frac{2d}{\alpha} + 1)$ for $d/2 < \alpha < \alpha_c$. However, for *quantum* systems with long-range interactions in the *"nonclassical" region* ($d/2 < \alpha < \alpha_c$), the quantum-classical correspondence is very subtle and there is no analytical expression for the critical exponents. Particularly, it is unclear whether the critical behavior of the $\mathbb{Z}_3$-symmetric *quantum* spin systems with long-range interactions is also consistent with the two-loop RG results of the *classical* Potts model with long-range interactions.

For *quantum* three-state Potts model systems with long-range power-law interactions, using nonperturbative DMRG, we found that there exists a critical value α_c in the long-range power-law interactions. When $\alpha < \alpha_c$, the RG flow ends in a stable long-range fixed point with varying critical exponents

ν, and when $\alpha > \alpha_c$, it ends in a short-range fixed point. These results for *quantum* three-state Potts model systems with long-range power-law interactions are in qualitative agreement with previous two-loop RG results for *classical* ϕ^3 theory [44]. More importantly, for the first time, we numerically determine the critical threshold of the long-range interaction power $\alpha_c \approx 1.43$ in a nonperturbative manner, which is more accurate than previous perturbative two-loop RG results $\alpha_c \sim 1.73$.

IV. CONCLUSION

To summarize, we investigate the critical behavior of the quantum Potts chain with long-range interactions through large-scale DMRG simulations. Using fidelity susceptibility as a diagnostic, we obtain a ground-state phase diagram between PM and Potts order phases. As the long-range interaction power increases, the location of the quantum critical point shifts to weaker external fields. The finite-size scaling of the fidelity susceptibility χ_F and the nature of the QPTs of the quantum Potts chain with long-range interaction are also investigated. Our numerical results show that there is a critical threshold α_c in the long-range interaction power, long-range fixed points are stable for $\alpha < \alpha_c$, and short-range fixed points are stable for $\alpha > \alpha_c$. These results are consistent with previous two-loop RG calculations from classical ϕ^3 theory, but the evolution of the critical point differs from the quantum Ising chains with long-range interaction [81]. In addition, for the first time, we determined the critical long-range interaction power $\alpha_c \approx 1.43$ in a nonperturbative way, which is more precise than the previous perturbative two-loop RG results $\alpha_c \sim 1.73$. Interesting future questions include the critical behavior and finite temperature effect in quantum four-state Potts chains with long-range interaction. Our work could shed new light on the interplay between long-range interactions (frustrated) and many-body physics.

ACKNOWLEDGMENTS

We thank Sheng Yang and Nicolo Defenu for helpful discussions and communication. Numerical simulations were carried out with the ITENSOR package [83]. We also thank the computational resources provided by the TianHe-1A supercomputer, the High Performance Computing Platform of Peking University, China. This work is supported by National Natural Science Foundation of China under Grant No.11935002, and the National 973 project under Grant No. 2021YF1400501. C.D. was supported by the National Science Foundation of China under Grant No. 11975024, and the Anhui Provincial Supporting Program for Excellent Young Talents in Colleges and Universities under Grant No. gxyqZD2019023.

APPENDIX A: FIDELITY SUSCEPTIBILITY FOR OTHER INTERACTION POWERS

In this section, we provide additional data to show fidelity susceptibility for other interaction powers.

As the same in the main text, on the one hand, fidelity susceptibility per site χ_L of the Potts chain with long-range interaction for $\alpha = 1.3$ (a), $\alpha = 1.35$ (b), $\alpha = 1.4$ (c), $\alpha = 1.5$ (d), $\alpha = 1.55$ (e), $\alpha = 1.6$ (f), $\alpha = 1.8$ (g), $\alpha = 2.0$ (h), and $L = 96, 120, 144, 156, 168, 192, 216, 240$ sites as a function of external transverse field f, are shown in Fig. 5. On the other hand, in order to determine critical α_c, we also show fidelity susceptibility per site for $\alpha = 1.41$ (a), $\alpha = 1.42$ (b), $\alpha = 1.43$ (c), $\alpha = 1.44$ (d), $\alpha = 1.45$ (e) in Fig. 6. We find that quantum critical points are shifted to lower values of f as long-range interaction power increases.

APPENDIX B: DATA COLLAPSES FOR OTHER INTERACTION POWERS

In this section, we provide additional data to show that the varying tendency of long-range correlation length exponents in the "nonclassical" region is consistent with theoretical analysis.

As the same in the main text, on the one hand, data collapse of fidelity susceptibility χ_F for the Potts chain with long-range interaction, $\alpha = 1.3$ (a), $\alpha = 1.35$(b), $\alpha = 1.4$ (c), $\alpha = 1.5$ (d), $\alpha = 1.55$ (e), $\alpha = 1.6$ (f), $\alpha = 1.8$ (g), $\alpha = 2.0$(h), and $L = 96, 120, 144, 156, 168, 192, 215, 240$ sites, are shown in Fig. 7. On the other hand, in order to determine critical α_c, we also show data collapse for $\alpha = 1.41$ (a), $\alpha = 1.42$ (b), $\alpha = 1.43$ (c), $\alpha = 1.44$ (d), and $\alpha = 1.45$ (e) in Fig. 8. The correlation length exponents are summarized in Table I. We clearly see that the varying tendency of correlation length exponents in the "nonclassical" region is consistent with the theoretical analysis.

APPENDIX C: QUANTUM ADIABATIC DIMENSION FITTING FOR OTHER INTERACTION POWERS

In this section, we provide additional data to extrapolate critical adiabatic dimensions for other long-range interaction powers.

As the same in the main text, on the one hand, the maximal of fidelity susceptibility per site $\chi_L(f_c(L)) = \chi_F(f_c(L))/L$ as a function of system sizes L for $\alpha = 1.3$ (a), $\alpha = 1.35$ (b), $\alpha = 1.4$ (c), $\alpha = 1.5$ (d), $\alpha = 1.55$ (e), $\alpha = 1.6$ (f), $\alpha = 1.8$ (g), $\alpha = 2.0$ (h), and $L = 96, 120, 144, 156, 168, 192, 216, 240$ sites, are shown in Fig. 9. On the other hand, in order to determine critical α_c, we also show the maximal of fidelity susceptibility per site for $\alpha = 1.41$ (a), $\alpha = 1.42$ (b), $\alpha = 1.43$ (c), $\alpha = 1.44$ (d), and $\alpha = 1.45$ (e) in Fig. 10. The critical adiabatic dimensions are summarized in the Table I. We clearly see that the varying tendency of critical adiabatic dimension in the "nonclassical" region is consistent with the theoretical analysis.

APPENDIX D: QUANTUM CRITICAL POINT FITTING FOR OTHER INTERACTION POWERS

In this section, we provide additional data to extrapolate accuracy critical points for other long-range interaction powers.

As the same in the main text, on the one hand, the finite-size scaling of pseudocritical point $f_c(L)$ as a function of inverse system sizes $1/L$ for $\alpha = 1.3$ (a), $\alpha = 1.35$ (b), $\alpha = 1.4$ (c), $\alpha = 1.5$ (d), $\alpha = 1.55$ (e), $\alpha = 1.6$ (f), $\alpha = 1.8$ (g), $\alpha = 2.0$ (h), and $L = 96, 120, 144, 156, 168, 192, 216, 240$

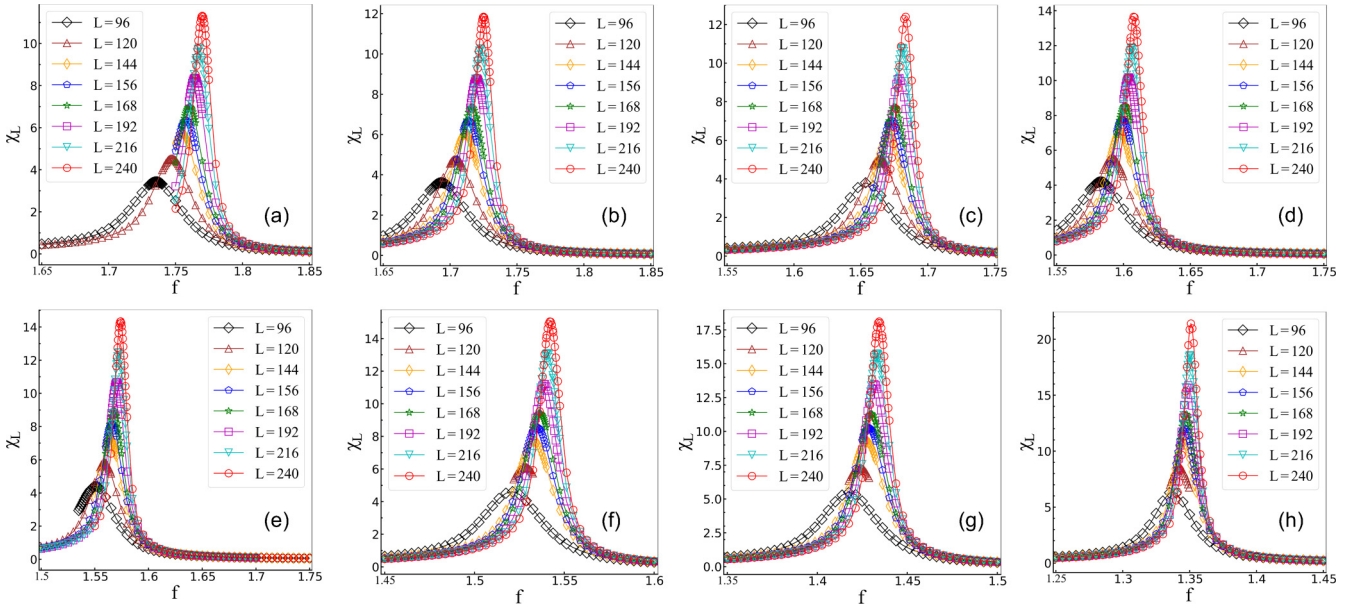

FIG. 5. Fidelity susceptibility per site χ_L of the Potts chain with long-range interaction for (a) $\alpha = 1.3$,(b) $\alpha = 1.35$, (c) $\alpha = 1.4$, (d) $\alpha = 1.5$, (e) $\alpha = 1.55$, (f) $\alpha = 1.6$, (g) $\alpha = 1.8$, (h) $\alpha = 2.0$, and $L = 96, 120, 144, 156, 168, 192, 216, 240$ sites as a function of external transverse field f; symbols denote finite-size DMRG results.

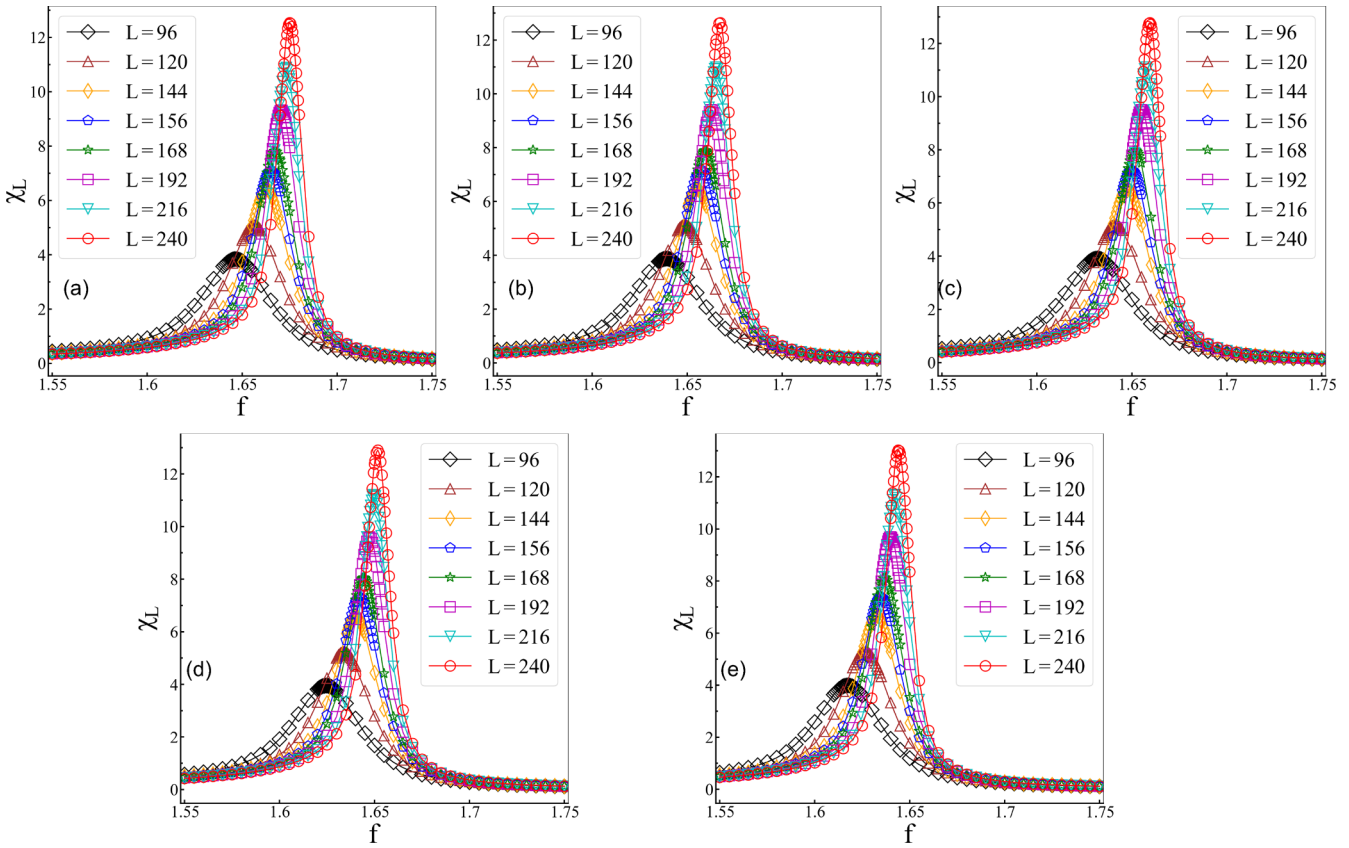

FIG. 6. Fidelity susceptibility per site χ_L of the Potts chain with long-range interaction for (a) $\alpha = 1.41$, (b) $\alpha = 1.42$, (c) $\alpha = 1.43$, (d) $\alpha = 1.44$, (e) $\alpha = 1.45$, and $L = 96, 120, 144, 156, 168, 192, 216, 240$ sites as a function of external transverse field f; symbols denote finite-size DMRG results.

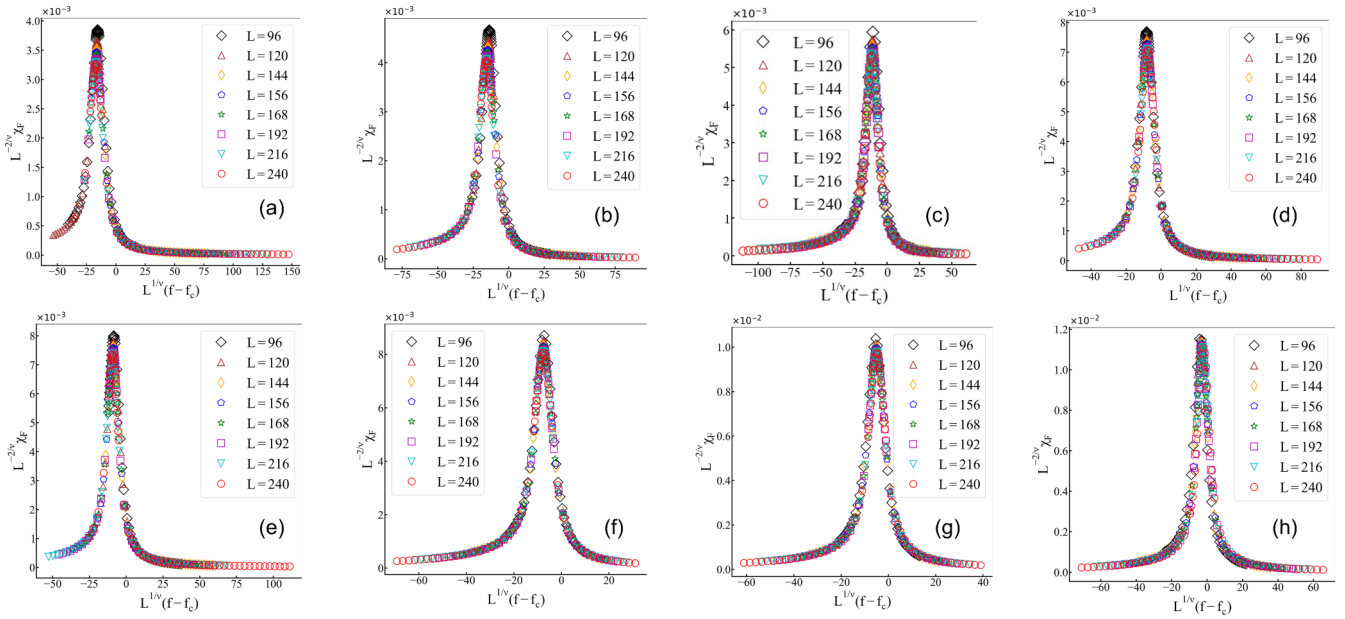

FIG. 7. Data collapse of fidelity susceptibility χ_F for the Potts chain with long-range interaction; symbols denote the finite-size DMRG results for (a) $\alpha = 1.3$, (b) $\alpha = 1.35$, (c) $\alpha = 1.4$, (d) $\alpha = 1.5$, (e) $\alpha = 1.55$, (f) $\alpha = 1.6$, (g) $\alpha = 1.8$, and (h) $\alpha = 2.0$, where the varying tendency of correlation length exponents in the "nonclassical" region is consistent with the theoretical analysis.

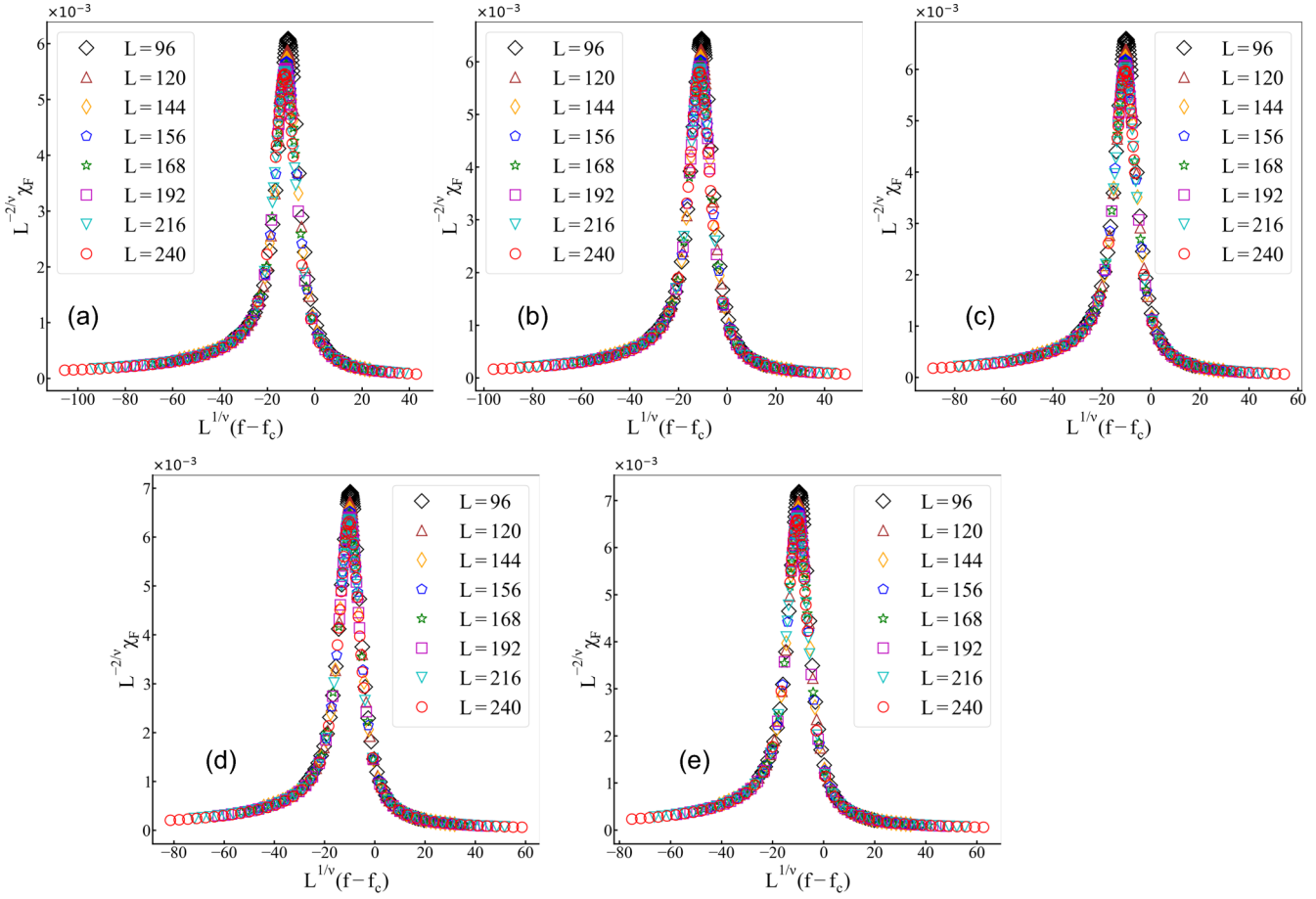

FIG. 8. Data collapse of fidelity susceptibility χ_F for the Potts chain with long-range interaction; symbols denote the finite-size DMRG results for (a) $\alpha = 1.41$, (b) $\alpha = 1.42$, (c) $\alpha = 1.43$, (d) $\alpha = 1.44$, and (e) $\alpha = 1.45$, where the varying tendency of correlation length exponents in the "nonclassical" region is consistent with the theoretical analysis.

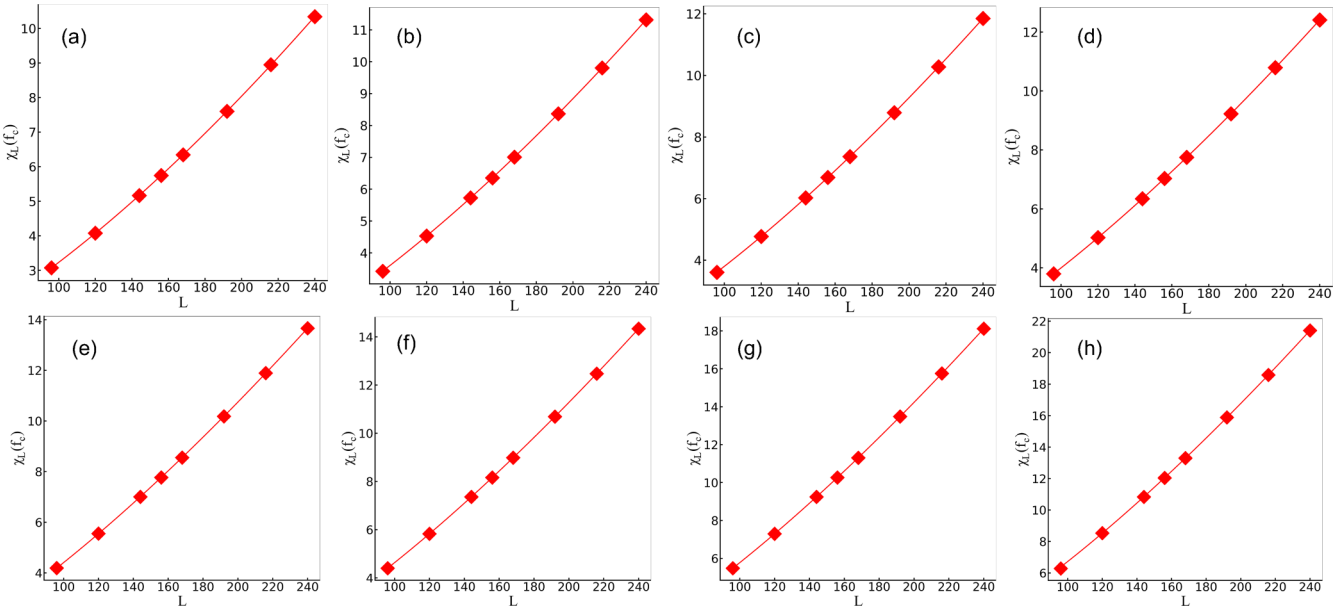

FIG. 9. The maximal of fidelity susceptibility per site $\chi_L(f_c(L)) = \chi_F(f_c(L))/L$ as a function of system sizes L for (a) $\alpha = 1.3$, (b) $\alpha = 1.35$, (c) $\alpha = 1.4$, (d) $\alpha = 1.5$, (e) $\alpha = 1.55$, (f) $\alpha = 1.6$, (g) $\alpha = 1.8$, and (h) $\alpha = 2.0$. We use polynomial fitting formula $\chi_L(f_c(L)) = L^{\mu-1}(c + dL^{-1})$.

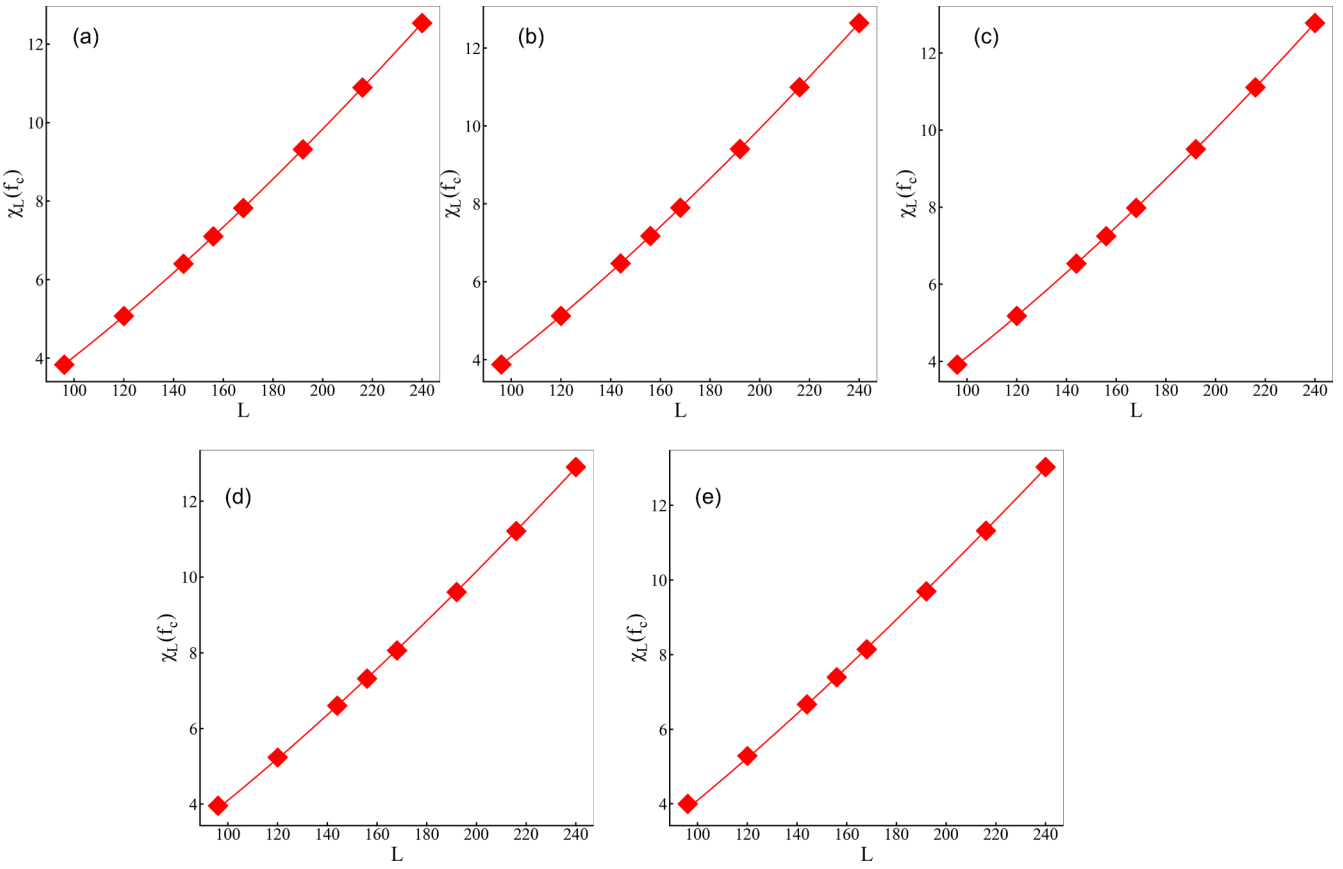

FIG. 10. The maximal of fidelity susceptibility per site as a function of system sizes L for (a) $\alpha = 1.41$, (b) $\alpha = 1.42$, (c) $\alpha = 1.43$, (d) $\alpha = 1.43$, and (e) $\alpha = 1.45$. We use polynomial fitting formula $\chi_L(f_c(L)) = L^{\mu-1}(c + dL^{-1})$.

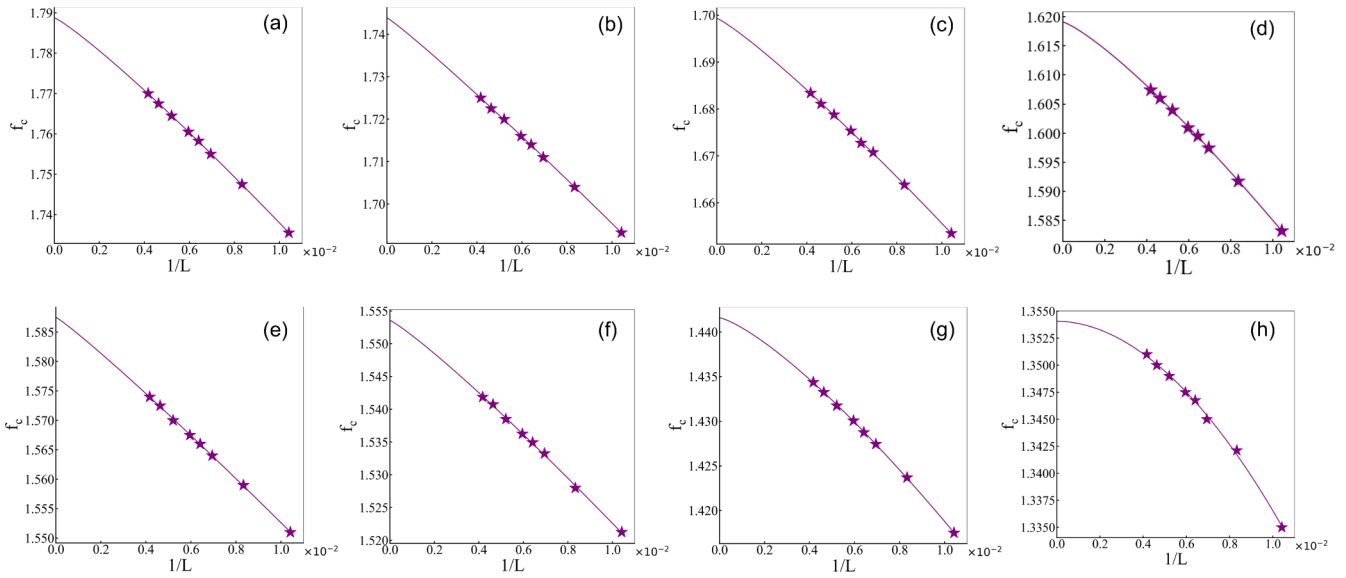

FIG. 11. The finite-size scaling of pseudocritical point $f_c(L)$ as a function of inverse system sizes $1/L$ for (a) $\alpha = 1.3$, (b) $\alpha = 1.35$, (c) $\alpha = 1.4$, (d) $\alpha = 1.5$, (e) $\alpha = 1.55$, (f) $\alpha = 1.6$, (g) $\alpha = 1.8$, and (h) $\alpha = 2.0$. We use polynomial fitting formula $f_c(L) = f_c^* + aL^{-1/\nu}$.

sites, are shown in Fig. 11. On the other hand, in order to determine critical α_c, we also show the finite-size scaling of pseudocritical point as a function of inverse system sizes for $\alpha = 1.41$ (a), $\alpha = 1.42$ (b), $\alpha = 1.43$ (c), $\alpha = 1.44$ (d), $\alpha = 1.45$ (e) in Fig. 12. The extrapolated critical points are summarized in Table I. We clearly see that the critical point f_c^* shifts to weaker values with increasing α.

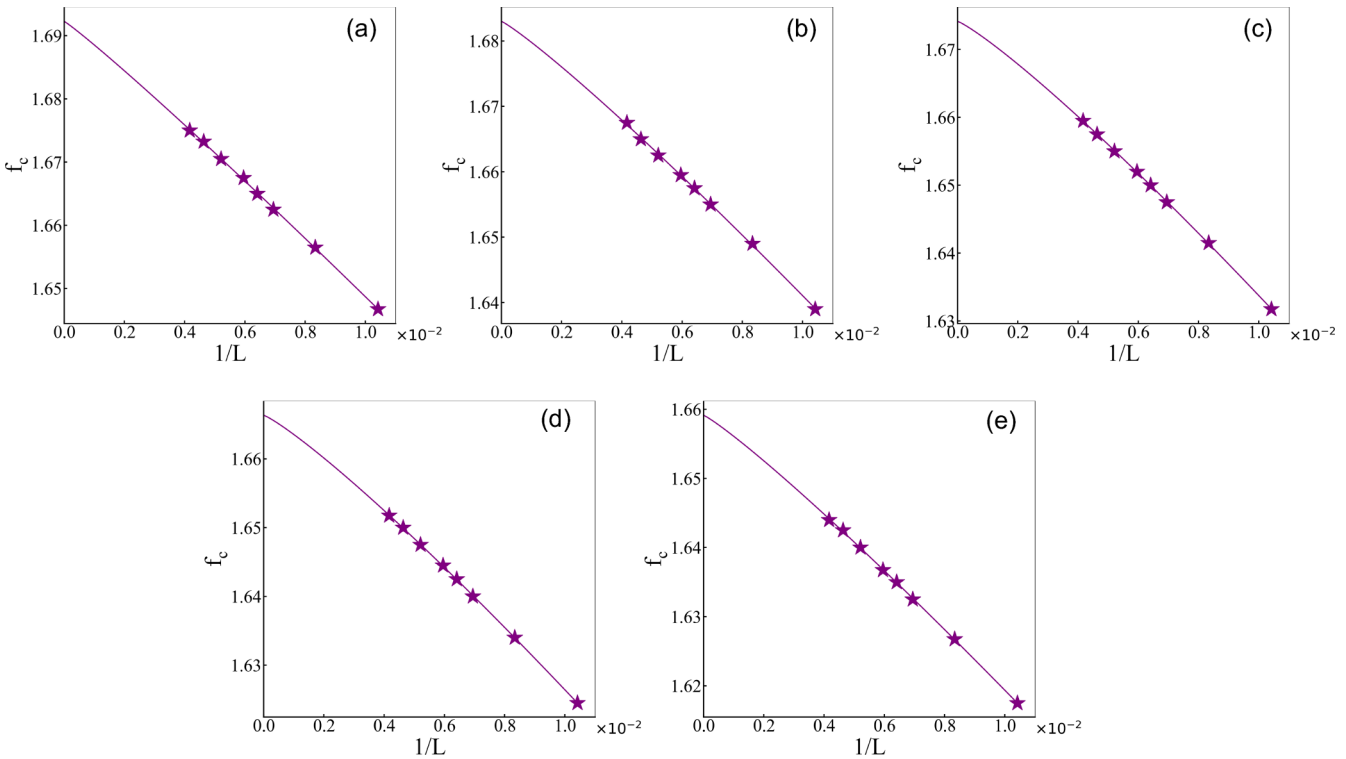

FIG. 12. The finite-size scaling of pseudocritical point $f_c(L)$ as a function of inverse system sizes $1/L$ for (a) $\alpha = 1.41$, (b) $\alpha = 1.42$, (c) $\alpha = 1.43$, (d) $\alpha = 1.44$, and (e) $\alpha = 1.45$. We use polynomial fitting formula $f_c(L) = f_c^* + aL^{-1/\nu}$.

[1] J. Cardy, *Scaling and Renormalization in Statistical Physics*, Vol. 5 (Cambridge University Press, Cambridge, 1996).

[2] C. Xu, Unconventional quantum critical points, Int. J. Mod. Phys. B **26**, 1230007 (2012).

[3] X.-J. Yu, P.-L. Zhao, S.-K. Jian, and Z. Pan, Emergent spacetime supersymmetry at disordered quantum critical points, Phys. Rev. B **105**, 205140 (2022).

[4] Z.-X. Guo, X.-J. Yu, X.-D. Hu, and Z. Li, Emergent phase transitions in a cluster Ising model with dissipation, Phys. Rev. A **105**, 053311 (2022).

[5] S. Sachdev, *Quantum Phase Transitions*, 2nd ed. (Cambridge University Press, Cambridge, 2011).

[6] M. Saffman, T. G. Walker, and K. Mølmer, Quantum information with Rydberg atoms, Rev. Mod. Phys. **82**, 2313 (2010).

[7] X.-L. Deng, D. Porras, and J. I. Cirac, Effective spin quantum phases in systems of trapped ions, Phys. Rev. A **72**, 063407 (2005).

[8] T. Lahaye, C. Menotti, L. Santos, M. Lewenstein, and T. Pfau, The physics of dipolar bosonic quantum gases, Rep. Prog. Phys. **72**, 126401 (2009).

[9] H. Ritsch, P. Domokos, F. Brennecke, and T. Esslinger, Cold atoms in cavity-generated dynamical optical potentials, Rev. Mod. Phys. **85**, 553 (2013).

[10] L. D. Carr, D. DeMille, R. V. Krems, and J. Ye, Cold and ultracold molecules: Science, technology and applications, New J. Phys. **11**, 055049 (2009).

[11] R. Blatt and C. F. Roos, Quantum simulations with trapped ions, Nat. Phys. **8**, 277 (2012).

[12] J. W. Britton, B. C Sawyer, A. C Keith, C.-C. J. Wang, J. K. Freericks, H. Uys, M. J. Biercuk, and J. J. Bollinger, Engineered two-dimensional Ising interactions in a trapped-ion quantum simulator with hundreds of spins, Nature (London) **484**, 489 (2012).

[13] R. Islam, C. Senko, W. C. Campbell, S. Korenblit, J. Smith, A Lee, E. E. Edwards, C.-C. J. Wang, J. K. Freericks, and C. Monroe, Emergence and frustration of magnetism with variable-range interactions in a quantum simulator, Science **340**, 583 (2013).

[14] P. Richerme, Z.-X. Gong, A. Lee, C. Senko, J. Smith, M. Foss-Feig, S. Michalakis, A. V. Gorshkov, and C. Monroe, Non-local propagation of correlations in quantum systems with long-range interactions, Nature (London) **511**, 198 (2014).

[15] P. Jurcevic, B. P. Lanyon, P. Hauke, C. Hempel, P. Zoller, R. Blatt, and C. F. Roos, Quasiparticle engineering and entanglement propagation in a quantum many-body system, Nature (London) **511**, 202 (2014).

[16] M. Song, J. Zhao, C. Zhou, and Z. Y. Meng, Dynamical properties of quantum many-body systems with long range interactions, arXiv:2301.00829.

[17] R. Verresen, M. D. Lukin, and A. Vishwanath, Prediction of Toric Code Topological Order from Rydberg Blockade, Phys. Rev. X **11**, 031005 (2021).

[18] R. Samajdar, D. G. Joshi, Y. Teng, and S. Sachdev, Emergent $\mathbb{Z}_2$ Gauge Theories and Topological Excitations in Rydberg Atom Arrays, Phys. Rev. Lett. **130**, 043601 (2023).

[19] G. Semeghini, H. Levine, A. Keesling, S. Ebadi, T. T. Wang, D. Bluvstein, R. Verresen, H. Pichler, M. Kalinowski, R. Samajdar *et al.*, Probing topological spin liquids on a programmable quantum simulator, Science **374**, 1242 (2021).

[20] R. Samajdar, W. W. Ho, H. Pichler, M. D. Lukin, and S. Sachdev, Quantum phases of Rydberg atoms on a kagome lattice, Proc. Natl. Acad. Sci. **118**, e2015785118 (2021).

[21] K. Slagle, Y. Liu, D. Aasen, H. Pichler, R. S. K. Mong, X. Chen, M. Endres, and J. Alicea, Quantum spin liquids bootstrapped from Ising criticality in Rydberg arrays, Phys. Rev. B **106**, 115122 (2022).

[22] Y. Cheng, C. Li, and H. Zhai, Variational approach to quantum spin liquid in a Rydberg atom simulator, New J. Phys. **25**, 033010 (2023).

[23] P. S. Tarabunga, F. M. Surace, R. Andreoni, A. Angelone, and M. Dalmonte, Gauge-Theoretic Origin of Rydberg Quantum Spin Liquids, Phys. Rev. Lett. **129**, 195301 (2022).

[24] R. Samajdar, W. W. Ho, H. Pichler, M. D. Lukin, and S. Sachdev, Complex Density Wave Orders and Quantum Phase Transitions in a Model of Square-Lattice Rydberg Atom Arrays, Phys. Rev. Lett. **124**, 103601 (2020).

[25] R. Samajdar, S. Choi, H. Pichler, M. D. Lukin, and S. Sachdev, Numerical study of the chiral $\mathbb{z}_3$ quantum phase transition in one spatial dimension, Phys. Rev. A **98**, 023614 (2018).

[26] S. Whitsitt, R. Samajdar, and S. Sachdev, Quantum field theory for the chiral clock transition in one spatial dimension, Phys. Rev. B **98**, 205118 (2018).

[27] M. Kalinowski, R. Samajdar, R. G. Melko, M. D. Lukin, S. Sachdev, and S. Choi, Bulk and boundary quantum phase transitions in a square Rydberg atom array, Phys. Rev. B **105**, 174417 (2022).

[28] M. J. O'Rourke and G. K.-L. Chan, Entanglement in the quantum phases of an unfrustrated Rydberg atom array, arXiv:2201.03189.

[29] E. Merali, I. J. S. De Vlugt, and R. G. Melko, Stochastic series expansion quantum Monte Carlo for Rydberg arrays, arXiv:2107.00766.

[30] K. Slagle, D. Aasen, H. Pichler, R. S. K. Mong, P. Fendley, X. Chen, M. Endres, and J. Alicea, Microscopic characterization of Ising conformal field theory in Rydberg chains, Phys. Rev. B **104**, 235109 (2021).

[31] G. Giudici, A. Angelone, G. Magnifico, Z. Zeng, G. Giudice, T. Mendes-Santos, and M. Dalmonte, Diagnosing Potts criticality and two-stage melting in one-dimensional hard-core boson models, Phys. Rev. B **99**, 094434 (2019).

[32] J. Alicea and P. Fendley, Topological phases with parafermions: theory and blueprints, Annu. Rev. Condens. Matter Phys. **7**, 119 (2016).

[33] P. Fendley, Parafermionic edge zero modes in $\mathbb{Z}_n$-invariant spin chains, J. Stat. Mech. (2012) P11020.

[34] E. O'Brien, E. Vernier, and P. Fendley, "Not-*A*", representation symmetry-protected topological, and Potts phases in an S_3-invariant chain, Phys. Rev. B **101**, 235108 (2020).

[35] Y. Zhuang, H. J. Changlani, N. M. Tubman, and T. L. Hughes, Phase diagram of the Z_3 parafermionic chain with chiral interactions, Phys. Rev. B **92**, 035154 (2015).

[36] E. O'Brien and P. Fendley, Self-dual S_3-invariant quantum chains, SciPost Phys. **9**, 088 (2020).

[37] X.-J. Yu, R.-Z. Huang, H.-H. Song, L. Xu, C. Ding, and L. Zhang, Conformal Boundary Conditions of Symmetry-Enriched Quantum Critical Spin Chains, Phys. Rev. Lett. **129**, 210601 (2022).

[38] A. Vaezi, Superconducting Analogue of the Parafermion Fractional Quantum Hall States, Phys. Rev. X **4**, 031009 (2014).

[39] W. Li, S. Yang, H.-H. Tu, and M. Cheng, Criticality in translation-invariant parafermion chains, Phys. Rev. B **91**, 115133 (2015).

[40] J. Wouters, F. Hassler, H. Katsura, and D. Schuricht, Phase diagram of an extended parafermion chain, SciPost Phys. Core **5**, 008 (2022).

[41] M. E. Fisher, S.-K. Ma, and B. G. Nickel, Critical Exponents for Long-Range Interactions, Phys. Rev. Lett. **29**, 917 (1972).

[42] M. Knap, A. Kantian, T. Giamarchi, I. Bloch, M. D. Lukin, and E. Demler, Probing Real-Space and Time-Resolved Correlation Functions with Many-Body Ramsey Interferometry, Phys. Rev. Lett. **111**, 147205 (2013).

[43] N. Defenu, A. Trombettoni, and S. Ruffo, Criticality and phase diagram of quantum long-range O(N) models, Phys. Rev. B **96**, 104432 (2017).

[44] W. K. Theumann and M. A. Gusmano, Critical exponents for φ^3-field models with long-range interactions, Phys. Rev. B **31**, 379 (1985).

[45] N. Defenu, T. Donner, T. Macrí, G. Pagano, S. Ruffo, and A. Trombettoni, Long-range interacting quantum systems, arXiv:2109.01063.

[46] N. Defenu, A. Trombettoni, and A. Codello, Fixed-point structure and effective fractional dimensionality for O(N) models with long-range interactions, Phys. Rev. E **92**, 052113 (2015).

[47] E. Brezin, G. Parisi, and F. Ricci-Tersenghi, The crossover region between long-range and short-range interactions for the critical exponents, J. Stat. Phys. **157**, 855 (2014).

[48] M. C. Angelini, G. Parisi, and F. Ricci-Tersenghi, Relations between short-range and long-range Ising models, Phys. Rev. E **89**, 062120 (2014).

[49] C. Behan, L. Rastelli, S. Rychkov, and B. Zan, Long-Range Critical Exponents Near the Short-Range Crossover, Phys. Rev. Lett. **118**, 241601 (2017).

[50] C. Behan, L. Rastelli, S. Rychkov, and B. Zan, A scaling theory for the long-range to short-range crossover and an infrared duality, J. Phys. A: Math. Theor. **50**, 354002 (2017).

[51] P. Francesco, P. Mathieu, and D. Sénéchal, *Conformal Field Theory* (Springer Science & Business Media, 2012).

[52] P. Ginsparg, Applied conformal field theory, arXiv:hep-th/9108028.

[53] W. C. Yu, S.-J. Gu, and H.-Q. Lin, Fidelity susceptibilities in the one-dimensional extended Hubbard model, arXiv:1408.2642 (2014).

[54] A. F. Albuquerque, F. Alet, C. Sire, and S. Capponi, Quantum critical scaling of fidelity susceptibility, Phys. Rev. B **81**, 064418 (2010).

[55] D. Schwandt, F. Alet, and S. Capponi, Quantum Monte Carlo Simulations of Fidelity at Magnetic Quantum Phase Transitions, Phys. Rev. Lett. **103**, 170501 (2009).

[56] W.-C. Yu, H.-M. Kwok, J. Cao, and S.-J. Gu, Fidelity susceptibility in the two-dimensional transverse-field Ising and xxz models, Phys. Rev. E **80**, 021108 (2009).

[57] G. Sun, A. K. Kolezhuk, and T. Vekua, Fidelity at Berezinskii-Kosterlitz-Thouless quantum phase transitions, Phys. Rev. B **91**, 014418 (2015).

[58] E. J. König, A. Levchenko, and N. Sedlmayr, Universal fidelity near quantum and topological phase transitions in finite one-dimensional systems, Phys. Rev. B **93**, 235160 (2016).

[59] B.-B. Wei, Fidelity susceptibility in one-dimensional disordered lattice models, Phys. Rev. A **99**, 042117 (2019).

[60] T. Lv, T.-C. Yi, L. Li, G. Sun, and W.-L. You, Quantum criticality and universality in the p-wave-paired Aubry-André-Harper model, Phys. Rev. A **105**, 013315 (2022).

[61] X.-J. Yu, S. Yang, J.-B. Xu, and L. Xu, Fidelity susceptibility as a diagnostic of the commensurate-incommensurate transition: A revisit of the programmable Rydberg chain, Phys. Rev. B **106**, 165124 (2022).

[62] G. Sun, B.-B. Wei, and S.-P. Kou, Fidelity as a probe for a deconfined quantum critical point, Phys. Rev. B **100**, 064427 (2019).

[63] Y.-T. Tu, I. Jang, P.-Y. Chang, and Y.-C. Tzeng, General properties of fidelity in non-Hermitian quantum systems with PT symmetry, arXiv:2203.01834.

[64] G. Sun, J.-C. Tang, and S.-P. Kou, Biorthogonal quantum criticality in non-Hermitian many-body systems, Front. Phys. **17**, 33502 (2022).

[65] S.-J. Gu and W. C. Yu, Spectral function and fidelity susceptibility in quantum critical phenomena, Europhys. Lett. **108**, 20002 (2014).

[66] S. Chen, L. Wang, Y. Hao, and Y. Wang, Intrinsic relation between ground-state fidelity and the characterization of a quantum phase transition, Phys. Rev. A **77**, 032111 (2008).

[67] W.-L. You and L. He, Generalized fidelity susceptibility at phase transitions, J. Phys.: Condens. Matter **27**, 205601 (2015).

[68] Y.-C. Tzeng, H.-H. Hung, Y.-C. Chen, and M.-F. Yang, Fidelity approach to Gaussian transitions, Phys. Rev. A **77**, 062321 (2008).

[69] S.-J. Gu, Fidelity approach to quantum phase transitions, Int. J. Mod. Phys. B **24**, 4371 (2010).

[70] S.-J. Gu, Fidelity susceptibility and quantum adiabatic condition in thermodynamic limits, Phys. Rev. E **79**, 061125 (2009).

[71] S.-J. Gu and H.-Q. Lin, Scaling dimension of fidelity susceptibility in quantum phase transitions, Europhys. Lett. **87**, 10003 (2009).

[72] Steven R. White, Density Matrix Formulation for Quantum Renormalization Groups, Phys. Rev. Lett. **69**, 2863 (1992).

[73] U. Schollwöck, The density-matrix renormalization group, Rev. Mod. Phys. **77**, 259 (2005).

[74] U. Schollwöck, The density-matrix renormalization group in the age of matrix product states, Ann. Phys. **326**, 96 (2011).

[75] F. Verstraete, D. Porras, and J. I. Cirac, Density Matrix Renormalization Group and Periodic Boundary Conditions: A Quantum Information Perspective, Phys. Rev. Lett. **93**, 227205 (2004).

[76] J. Sólyom and P. Pfeuty, Renormalization-group study of the Hamiltonian version of the Potts model, Phys. Rev. B **24**, 218 (1981).

[77] R.-Z. Huang and S. Yin, Nonequilibrium critical dynamics in the quantum chiral clock model, Phys. Rev. B **99**, 184104 (2019).

[78] H. J. Lipkin, N. Meshkov, and A. J. Glick, Validity of many-body approximation methods for a solvable model: (i). exact solutions and perturbation theory, Nucl. Phys. **62**, 188 (1965).

[79] B. Damski, Fidelity approach to quantum phase transitions in quantum Ising model, in *Quantum Criticality in Condensed Matter: Phenomena, Materials and Ideas in Theory and Experiment* (World Scientific, Singapore, 2016), pp. 159–182.

[80] A. W. Sandvik, Computational studies of quantum spin systems, in AIP Conference Proceedings, Vol. 1297 (American Institute of Physics, Melville, 2010), pp. 135–338.

[81] G. Sun, Fidelity susceptibility study of quantum long-range antiferromagnetic Ising chain, Phys. Rev. A **96**, 043621 (2017).

[82] Z. Zhu, G. Sun, W.-L. You, and D.-N. Shi, Fidelity and criticality of a quantum Ising chain with long-range interactions, Phys. Rev. A **98**, 023607 (2018).

[83] M. Fishman, S. R. White, and E. M. Stoudenmire, The ITensor software library for tensor network calculations, SciPost Phys. Codebases 004 (2022).